Remote control of renal physiology by the intestinal neuropeptide pigment-dispersing factor in *Drosophila*

Aaron D. Talsma[a], Christo P. Christov[b], Ana Terriente-Felix[b,1], Gerit A. Linneweber[b], Daniel Perea[b], Matthew Wayland[b], Orie T. Shafer[a,2], and Irene Miguel-Aliaga[b,2]

[a]Department of Molecular, Cellular, and Developmental Biology, University of Michigan, Ann Arbor, MI 48109; and [b]Department of Zoology, University of Cambridge, Cambridge CB2 3EJ, United Kingdom

Edited* by Michael Rosbash, Howard Hughes Medical Institute, Waltham, MA, and approved June 12, 2012 (received for review January 5, 2012)

The role of the central neuropeptide pigment-dispersing factor (PDF) in circadian timekeeping in *Drosophila* is remarkably similar to that of vasoactive intestinal peptide (VIP) in mammals. Like VIP, PDF is expressed outside the circadian network by neurons innervating the gut, but the function and mode of action of this PDF have not been characterized. Here we investigate the visceral roles of PDF by adapting cellular and physiological methods to the study of visceral responses to PDF signaling in wild-type and mutant genetic backgrounds. We find that intestinal PDF acts at a distance on the renal system, where it regulates ureter contractions. We show that PdfR, PDF's established receptor, is expressed by the muscles of the excretory system, and present evidence that PdfR-induced cAMP increases underlie the myotropic effects of PDF. These findings extend the similarities between PDF and VIP beyond their shared central role as circadian regulators, and uncover an unexpected endocrine mode of myotropic action for an intestinal neuropeptide on the renal system.

intestine | tubule | enteric | nervous system

The gastrointestinal tract is an important signaling center that, through its production of systemic or neural signals, can have profound effects on other organs (1, 2). In some cases, the nature of these signals and their modes of action are beginning to be elucidated; for example, postprandial release of cholecystochinin hormone from the duodenum has been shown to reduce appetite through its action on the vagus nerve, and intestinal glucagon-like peptide 1 can regulate pancreatic insulin secretion in response to glucose intake (1, 3). However, the contribution of intestinal signals to the maintenance of homeostasis is likely to involve many more molecules and target tissues, as highlighted by our incomplete understanding of the amelioration of diabetes and hypertension resulting from bariatric surgery, or the contribution of deregulated intestinal signaling to conditions such as diabetes and obesity (1, 2).

Several mammalian families of hormones are conserved in insects (4, 5), some of which are present in the digestive tract, where they are produced by endocrine cells of the gut epithelium or by neurons innervating the gut (6, 7). Previous work has revealed myotropic effects for some of these peptides on explanted viscera (5, 7–9). These studies have typically made use of large insects that, although amenable to physiological study, cannot be easily manipulated genetically. This difficulty has precluded further investigation of the specific sites of release and cellular modes of action of these peptides.

Vasoactive intestinal polypeptide (VIP) is a 28-aa peptide hormone produced in many areas of the human body, including the brain and digestive tract (3, 10). VIP signals through two G protein-coupled receptors (GPCRs), VPAC1 and VPAC2, which are also widely expressed in the CNS and the smooth muscles of the digestive and urogenital tracts (11, 12). Genetic experiments have uncovered a broad range of functions for VIP and its receptors, including the regulation of smooth-muscle contraction in the digestive and excretory systems and an important role in circadian timekeeping in the suprachiasmatic nuclei of the hypothalamus (3, 10, 12). This latter function is strikingly similar to that of the 18-aa pigment-dispersing factor (PDF) in the *Drosophila* brain (13); the loss of PDF in flies and VIP in mice results in the inability to maintain strong, normally paced locomotor rhythms (14, 15), and both peptides mediate communication between neurons of the circadian clock network (16–20). These similarities are molecular as well as functional; VPAC2 and PdfR, the PDF receptor in flies, are both type II secretin-like receptors (21–23). The peripheral roles of *Drosophila* PDF and its receptor have not been investigated.

Here we investigate the visceral functions of PDF in *Drosophila*. By revealing a myotropic function for PDF and PdfR in the regulation of renal musculature, we uncover an endocrine mode of action for PDF and identify further similarities between PDF and mammalian VIP beyond the circadian clock. More generally, our findings point to an unexpected endocrine function for a gut-derived peptide in the regulation of renal function.

Results

Central Efferent PDF Neurons Innervate the Intestine of *Drosophila* Larvae and Adults. As part of our ongoing characterization of the signals exchanged between the nervous and digestive system in *Drosophila* (24), we turned our attention to the PDF neurites of the digestive tract, which project from neuronal cell bodies previously described for both the blowfly and *Drosophila* (7), but whose visceral targets have not been reported for adult *Drosophila* in detail (25). In addition to the expression of PDF by brain clock neurons, PDF is expressed by neurons in the ventral nerve cord (VNC) (25, 26) that do not express clock genes (7, 20). Expression analyses using a *PDF-GAL4* reporter and an antibody against the PDF propeptide confirmed these previous reports, and revealed that the number of PDF^+ efferent neurons is variable and age-dependent. Of the six to eight PDF^+ neurons in the posterior abdominal segments of the larval VNC (Fig. 1*A*), four to eight persist in adults (Fig. 1*B*), wherein two populations of PDF^+ neurons are apparent: three to four cell bodies that strongly express PDF, and one to four additional neurons displaying weak PDF expression (Fig. 1*E*). In young adults (<1 wk old), we find 3.6 ± 0.5 strongly expressing PDF neurons and 2.8 ± 2.3 weak ones. In older adults (>2 wk old), 3.9 ± 0.4 strongly expressing and only 0.9 ± 1.4 weakly expressing neurons are apparent.

The size and position of the abdominal PDF (ab-PDF) neurons were reminiscent of the gut-innervating MP1 and dMP2 neurons, which express the transcription factor Odd-skipped (27, 28). An anti–Odd-skipped antibody confirmed that the ab-PDF neurons are the MP1 and dMP2 neurons of segments A8 and A9 (Fig. 1*D*). Analysis of adult ab-PDF axons revealed visceral innervation similar to that of the blowfly (25). Ab-PDF neurons

Author contributions: A.D.T., A.T.-F., O.T.S., and I.M.-A. designed research; A.D.T., C.P.C., A.T.-F., G.A.L., D.P., O.T.S., and I.M.-A. performed research; A.D.T., C.P.C., A.T.-F., G.A.L., M.W., O.T.S., and I.M.-A. analyzed data; and O.T.S. and I.M.-A. wrote the paper.

The authors declare no conflict of interest.

*This Direct Submission article had a prearranged editor.

Freely available online through the PNAS open access option.

[1]Present address: Department of Physiology, Development, and Neuroscience, University of Cambridge, Cambridge CB2 3EG, United Kingdom.

[2]To whom correspondence may be addressed. E-mail: oshafer@umich.edu or im307@cam.ac.uk.

This article contains supporting information online at www.pnas.org/lookup/suppl/doi:10.1073/pnas.1200247109/-/DCSupplemental.

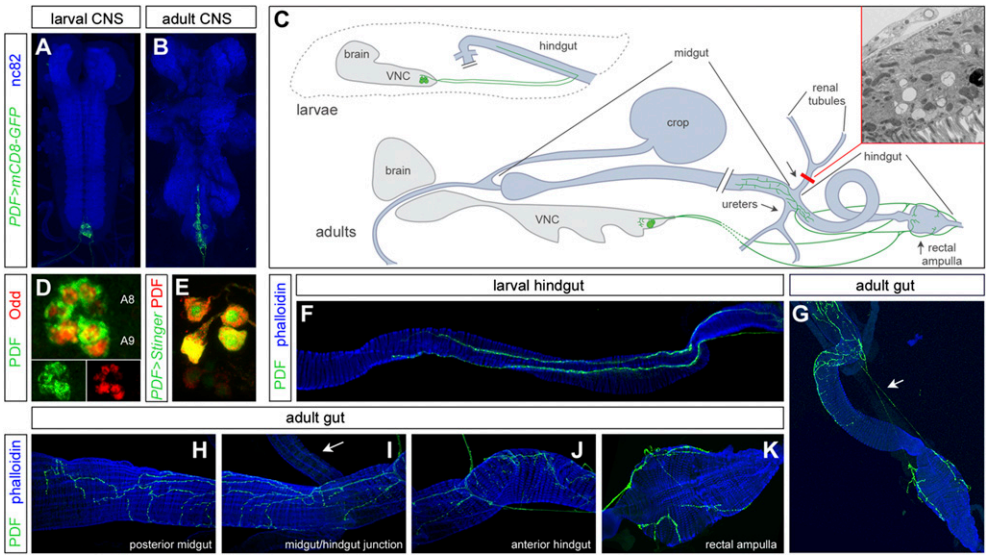

Fig. 1. The ab-PDF neurons innervate the larval and adult intestine. (*A*) Six to eight *PDF-GAL4*$^{+}$ efferent neurons are apparent in the two posterior-most segments of the larval VNC. (*B*) Four to eight of these neurons persist in the adult VNC. In *A* and *B*, nc82 is used as a general neuropil marker. (*C*) Summary of the innervation of the larval and adult intestine by the ab-PDF neurons. The CNS is in gray, the digestive tract is displayed in light blue. Only the hindgut is shown in larvae and only half of the cell bodies are displayed. The electron micrograph boxed in red shows a cross-section of the ureters at the level indicated by the red line. A tracheal terminal and a muscle cell are apparent, but no neurites or neuronal cell bodies are present (see Fig. S1 for additional micrographs). (*D*) The ab-PDF neurons in the larval A8 and A9 posterior segments are Odd^{+}. (*E*) In the adult VNC, four neurons strongly express both PDF (in red) and *PDF-GAL4* (in green, visualized with the nuclear *UAS-Stinger*) (51). One to four weakly expressing neurons (posterior to the other neurons in this image) are apparent in some CNSs. (*F*) PDF innervation of the larval hindgut. Two parallel fibers extend along the hindgut muscles. (*G–K*) PDF innervation of the adult intestine. (*G*) Connection (arrow) between the rectal ampulla branches and the gut terminals. (*H*) Innervation of the posterior midgut. (*I*) Innervation of the midgut/hindgut junction. The ureter (arrow) is not innervated. (*J*) Innervation of the anterior hindgut. (*K*) PDF neurites on the rectal ampulla. In *F–K*, phalloidin is used to visualize the gut muscles. The images in *A*, *B*, *F*, and *G* were captured using a 10× objective; *D*, *E*, and *H–K* were captured using a 63× objective.

form two nerves that reach the posterior hindgut and extend aborally to orally along the sides of the hindgut in larvae (Fig. 1 *C* and *F*). PDF^{+} varicosities are apparent throughout the length of these fibers. In adults, the two PDF^{+} nerves form complex arbors that populate the posterior midgut and anterior hindgut (Fig. 1 *C* and *H–J*). A subset of PDF neurites branch off from these main fibers to project to the rectum (Fig. 1 *C*, *G*, and *K*). Besides the CNS and digestive tract, no PDF immunoreactivity was apparent in other adult tissues. Absence of innervation of the renal tubules (Fig. 1*I*) was further confirmed using transmission electron microscopy (Fig. 1*C* and Fig. S1). Thus, the only visceral site of PDF innervation is the posterior intestine, which is supplied by the central neurosecretory MP1 and dMP2 lineages.

PDF Induces Ureter Contractions but Has No Acute Effects on Intestinal Motility. The intestinal innervation of the ab-PDF neurons prompted us to investigate if PDF modulates visceral contractions. We adapted the ex vivo motility assays used in larger insects to quantify contractions in the smaller adult viscera of *Drosophila* (Fig. S2), and asked if PDF caused changes in visceral contraction. Under our initial experimental conditions, viscera from wild-type Canton S flies displayed low basal contraction rates (Fig. 2*D*, Fig. S3*A*, and Movies S1 and S2), and a range of PDF concentrations resulted in no significant changes in midgut or hindgut contractions (Fig. 2 *A* and *B*, and Fig. S3*A*). Unexpectedly, PDF caused dose-dependent increases in ureter contraction rate (Fig. 2 *A* and *B*, and Movie S3), a neighboring tissue not directly innervated by PDF neurons (Fig. 1 *C* and *I*, and Fig. S1). In *Drosophila*, each set of renal tubules converge onto a muscular ureter, which controls the flow of urine to the gut (Fig. 1 *C* and *I*) (29, 30). For male ureters, PDF concentrations greater than 10^{-9} M caused contraction rates that were significantly higher than those of vehicle controls (Fig. 2*A*). For females, PDF concentrations greater than 10^{-8} M induced contraction rates that were significantly higher than vehicle controls (Fig. 2*B*). The EC_{50} of the PDF dose–response curve for ureter contraction rates was 2.406×10^{-9} M PDF for males and 7.214×10^{-9} M PDF for females.

These experiments suggested that, although ab-PDF neurons innervate the digestive tract, PDF does not alter intestinal peristalsis, but rather stimulates ureter contraction. We repeated these experiments on viscera dissected from CO_2 anesthetized flies into room temperature hemolymph-like saline (HL3), to rule out chilling and the relatively high K^{+} concentrations associated with the ice-cold Ringer's as the reason for the lack of PDF effects on the gut. This increased basal visceral contraction rates (Fig. 2*E* and Fig. S3*B*), allowing us to test the ability of PDF to contract or relax the digestive tract. Under these conditions, PDF application neither increased nor reduced gut contraction rates (Fig. S3*B*) but significantly increased ureter contraction rates (Fig. 2*C*). Thus, PDF has a specific myotropic effect on the renal system, suggesting an endocrine mode of action for the gut-innervating ab-PDF neurons.

PdfR Is Expressed in Ureter Muscles and Is Required for PDF's Effects on Ureters. In its role as a regulator of circadian locomotor rhythms, PDF signals through PdfR, a GPCR encoded by *CG13758* (21–23). To test if *PdfR* is required for PDF's effects on ureters, we compared the PDF responses of adult viscera dissected from the wild-type w^{1118} strain and the *PdfR* mutants $PdfR^{3369}$ and $PdfR^{5304}$ (21). Ureters from w^{1118} control flies displayed large increases in contraction rates when treated with 10^{-7} M PDF. In contrast, neither *PdfR* mutant displayed increased ureter contraction rates in response to PDF (Fig. 2*D*). This same pattern held true for w^{1118} and $PdfR^{5304}$ ureters dissected under warm HL3 (Fig. 2*E*).

These results suggested that PdfR acts within the ureter to trigger PDF-induced contractions. We therefore mapped the visceral expression of *PdfR* using in situ hybridization, as anti-PdfR sera are unsuitable for immunocytochemistry (31). *PdfR* RNA is present in both larval and adult ureter circular muscles (Fig. 3 *A*, *B*, *D*, and *E*). Weaker expression in midgut and hindgut muscles could be observed in some, but not all, digestive tracts. These *PdfR* RNA signals were absent in $PdfR^{5304}$ mutants (Fig. 3 *C* and *F*). We also compared *PdfR* RNA abundance relative to the housekeeping gene *Rpl32* in distal renal tubules, ureters, and midguts using real-time PCR. Consistent with our in situ results, ureters expressed relatively high levels of *PdfR* RNA compared with distal renal tubules and midguts, although *PdfR* RNA expression was detectable in all three of these visceral tissues (Fig. S4). Thus, anatomical, molecular, and physiological evidence all indicate a role for PdfR acting in the ureter muscles to mediate the myotropic effects of PDF on the renal system.

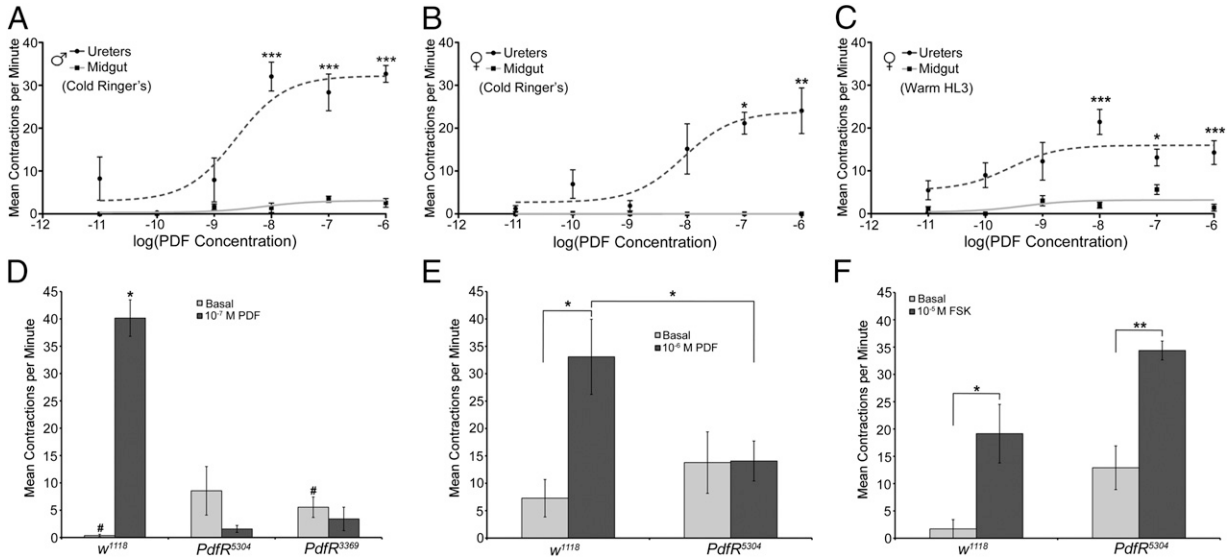

Fig. 2. PDF induces PdfR-dependent ureter contractions. (*A*) Dose–response curves for PDF on the contraction rates of male Canton S (wild-type) midguts and ureters dissected in cold Ringer's with contractions expressed as contractions per minute (cpm ± SEM). Mean basal contraction rates were 3.09 ± 1.72 cpm for the ureters and 0 ± 0 cpm for midguts. Mean contraction rates for vehicle controls were 0.60 ± 0.34 cpm for ureters and 0 ± 0 cpm for midguts. The EC_{50} was 2.41×10^{-9} M PDF. (*B*) Dose–response curves for PDF on contraction rates of female Canton S midguts and ureters. Mean basal contraction rates were 2.38 ± 1.43 cpm for the ureters and 0.38 ± 0.28 cpm for midguts. Mean contraction rates for vehicle controls were 4.07 ± 1.82 cpm for ureters and 1.93 ± 1.20 cpm for midguts. The EC_{50} was 8.72 ± 10^{-9}. (*C*) Dose–response curves for female wild-type midguts and ureters dissected in warm HL3. Mean basal contraction rates were 2.48 ± 0.58 cpm for the ureters and 0.45 ± 0.13 cpm for midguts. Mean contraction rates for vehicle controls were 2.08 ± 1.66 cpm for ureters and 0 ± 0 cpm for midguts. The EC_{50} was 2.71×10^{-10} M PDF. (*D*) Comparison of PDF effects on ureter contraction rates from wild-type (w^{1118}) and *PdfR* mutant ($PdfR^{5304}$ and $PdfR^{3369}$) viscera prepared using cold Ringer's solution. For wild-type ureters, the addition of 10^{-7} M PDF caused a significant increase in ureter contraction rate ($P < 0.001$). No significant increase in contraction rate was seen in either *PdfR* mutant ($PdfR^{5304}$: $P = 0.4688$; $PdfR^{3369}$: $P = 0.4375$). *PdfR* mutants displayed higher basal ureter contraction rates compared with w^{1118} ureters, but this difference was statistically significant only for $PdfR^{3369}$ [indicated by pound (#) signs, $PdfR^{5304}$: $P = 0.0623$; $PdfR^{3369}$: $P = 0.0497$]. (*E*) The effects of 10^{-6} M PDF on the ureters of w^{1118} and $PdfR^{5304}$ viscera prepared using warm HL3. PDF caused significant increases in the contractions rates of w^{1118} ureters compared with basal rates ($P = 0.0313$) and to PDF-treated $PdfR^{5304}$ tubules ($P = 0.0230$). There was no significant difference in basal and PDF-treated contraction rates of $PdfR^{5304}$ ureters ($P = 0.9340$). (*F*) The effects of FSK on the ureters of wild-type (w^{1118}) and $PdfR^{5304}$ viscera dissected using warm HL3. Wild-type ureters responded to 10 μM FSK with a significant increase in contraction rate compared with basal rates ($P = 0.013$), as did the ureters of $PdfR^{5304}$ viscera ($P = 0.0313$). On all graphs the error bars = SEM. For *A* and *B*, significance was tested by a Mann–Whitney *U* test comparing the contraction rates of PDF-treated viscera to those of vehicle-treated viscera (0.1% DMSO). In *D*–*F* PDF-treated contraction rates were compared with basal rates using paired-sample Wilcoxon signed rank tests. *$P < 0.05$, **$P < 0.01$, and ***$P < 0.001$).

cAMP Increases Underlie the Visceral Effects of PDF. In central brain neurons, PdfR signals through increases in cAMP (23, 31). To investigate if ureter muscles display cAMP increases in response to PDF, we conducted cAMP imaging using the FRET sensor Epac1-camps, which has been used in the brain to measure PDF-induced cAMP increases (31). Epac1-camps displays a loss of YFP/CFP FRET when cAMP levels rise (32). We expressed *UAS-Epac1-camps* using *Mef2-GAL4*: an enhancer trap that reports the expression of *myocyte enhancer factor 2*, a transcription factor expressed by muscle cells (33), resulting in sensor expression in the ureter musculature (Fig. S5). The ratiometric nature of the sensor allowed for FRET measurements in moving ureters (Movies S4 and S5). Wild-type ureter muscles showed significant FRET loss in response to 10^{-6} M PDF (Fig. 4 *A*, *C*, and *D*), consistent with PDF-induced cAMP increases in the ureter muscles. At doses of 10^{-7} M PDF, a concentration that consistently elicits ureter contractions (Fig. 2 *A* and *B*), only a subset of ureter muscles responded with significant FRET changes (Fig. 4*B*). This discrepancy might reflect a limitation of the sensor whose affinity for cAMP must be high enough to respond to physiologically relevant cAMP concentrations, but low enough not to grossly interfere with cellular physiology and signaling. We next performed Epac1-camps imaging on the ureter muscles of $PdfR^{5304}$;*UAS-Epac1-camps*/*Mef2-GAL4* male flies. The muscles of $PdfR^{5304}$ mutant ureters did not respond to 10^{-6} or 10^{-7} M PDF (Fig. 4 *E*–*H*). Thus, the cAMP response of the ureter muscles to PDF requires PdfR.

These results suggested that PDF affects ureter motility through cAMP increases. We asked if elevating cAMP would induce ureter contractions using forskolin (FSK), a direct activator of adenylate cyclases (34). FSK application caused significant increases in ureter contractions (Fig. 2*F*). Thus, increasing cAMP resulted in increased ureter contractions. FSK also caused significant increases in midgut contraction rates, but only in preparations dissected in warm HL3 buffer (Fig. S3*C*). This finding is consistent with previous work finding that cAMP signaling stimulates gut contractions in *Acheta* (35) and indicates that dissected guts were capable of contraction, lending further support to the lack of myotropic effects of PDF on the gut.

These results indicate that PDF-triggered PdfR activation in ureters results in cAMP increases, and support a model in which PdfR signaling in ureter muscles induces contractions through cAMP increases.

PdfR Expression in the Visceral Muscles of *PdfR* Mutants Rescues PDF-Induced Renal Motility. We next asked if PDF responsiveness could be conferred on $PdfR^{5304}$ ureters by rescuing PdfR expression in visceral muscles using *UAS-*$PdfR^{16L}$, which is capable of rescuing the geotaxic defects displayed by *PdfR* mutants (23) and confers PDF responsiveness to neurons that do not typically respond to PDF (31). We first used *Mef2-GAL4* (Fig. 5*A*) to reinstate *PdfR* expression in ureter muscles. The $PdfR^{5304}$;*UAS-*$PdfR^{16L}$/*Mef2-GAL4* rescue line displayed a significantly higher frequency of ureter contractions than $PdfR^{5304}$;*UAS-*$PdfR^{16L}$/+ controls in the presence of 10^{-6} M PDF (Fig. 5*B*) ($P = 0.0021$), with rates approaching those of wild-type ureters. The Mef2-rescue line also displayed mean contraction rates that were higher than those of $PdfR^{5304}$;*Mef2-GAL4*/+ controls, but because of the relatively high contraction rate of a single $PdfR^{5304}$;*Mef2-GAL4*/+ preparation, this difference was not statistically significant ($P = 0.0861$). The *24B-GAL4* line drives expression

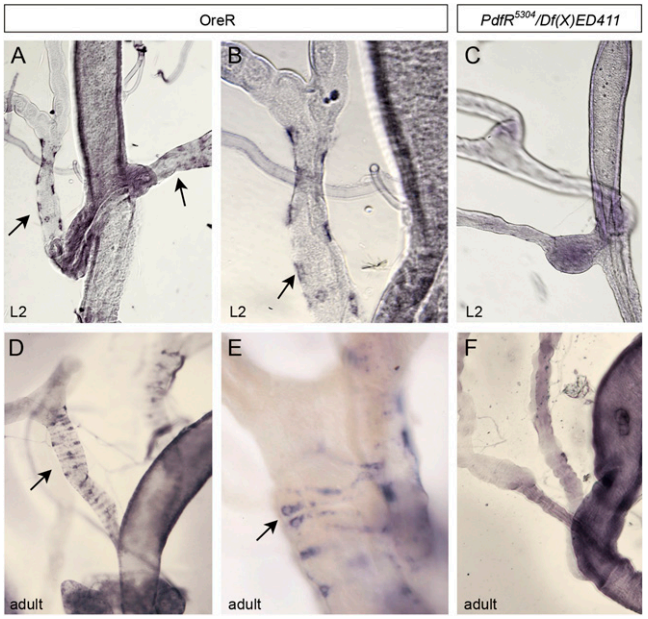

Fig. 3. PdfR mRNA is expressed in ureter circular muscles. (*A* and *B*) In situ hybridization reveals expression of *PdfR* RNA in wild-type (Oregon-R) larval ureters (*A*, arrows). The perinuclear and banded signal is characteristic of circular muscle expression (*B*, arrow). (*C*) No signal is apparent in *PdfR* mutant larval ureters. (*D* and *E*) *PdfR* expression in adult Oregon-R ureters (arrows). (*F*) The *PdfR* signal is absent in *PdfR* mutant adult ureters. *A*, *C*, *D* and *F* were captured using a 10× objective; *B* and *E* were captured using a 20× objective.

in the ureter musculature (Fig. 5*C*) and the $PdfR^{5304}$;*UAS-*$PdfR^{16L}$/+;*24B-GAL4*/+ rescue line displayed a significantly higher frequency of ureter contractions than the $PdfR^{5304}$;;*24B-GAL4*/+ ($P = 0.0087$) and $PdfR^{5304}$;*UAS-*$PdfR^{16L}$/+ ($P = 0.0032$) controls in the presence of 10^{-6} M PDF (Fig. 5*D*). Thus, *24B-GAL4*-driven *PdfR* expression rescued the PDF responsiveness of $PdfR^{5304}$ ureters. No such rescue was observed when *UAS-*$PdfR^{16L}$ was expressed using *MyoIA-GAL4*, an enhancer trap for the *myosin 1A* gene, which is expressed in epithelial cells of the midgut and proximal tubule (36), but not in the muscles of the ureter (Fig. 5 *E* and *F*). Thus, the GPCR required for PDF's role in central circadian timekeeping also mediates a peripheral action of this peptide.

Excitation of Visceral PDF Axons Stimulates Ureter Contractions. The lack of renal PDF innervation, together with the experiments described above, indicate that PDF from the ab-PDF neurons acts at a distance to stimulate ureter contractions. To test this model, we adapted the use of the *Drosophila* TrpA1 (dTrpA1) heat-sensitive channel, which renders neurons excitable by high temperature pulses (37), to excite visceral PDF axons in explanted viscera. Heat activation of *PDF-GAL4*-driven dTrpA1 did not affect gut peristalsis significantly, but led to a significant increases in ureter contraction rates (Fig. 6, and Movies S6 and S7). Because the axons of the abdominal gut-innervating PDF neurons were the only dTrpA1-expressing neurites present in this preparation, we conclude that excitation of the ab-PDF neurons is sufficient to stimulate ureter contractions without affecting midgut motility.

Discussion

***Drosophila* PDF and Mammalian VIP: Striking Similarities Beyond the Circadian Clock Network.** Striking similarities have been found between fly PDF and mammalian VIP in the generation of daily behavioral rhythms (10, 13). Outside the central clock, mammalian VIP and its related ligand PACAP (pituitary adenylate cyclase activating peptide) act on smooth-muscle receptors in a variety of internal organs, including those of the lower urinary tract (39–43). Our findings of broad visceral PdfR expression and a function for PDF signaling in the regulation of visceral muscle contraction extend the similarities between these peptides and their receptors beyond the central clock. The PdfR-expressing circular muscles of

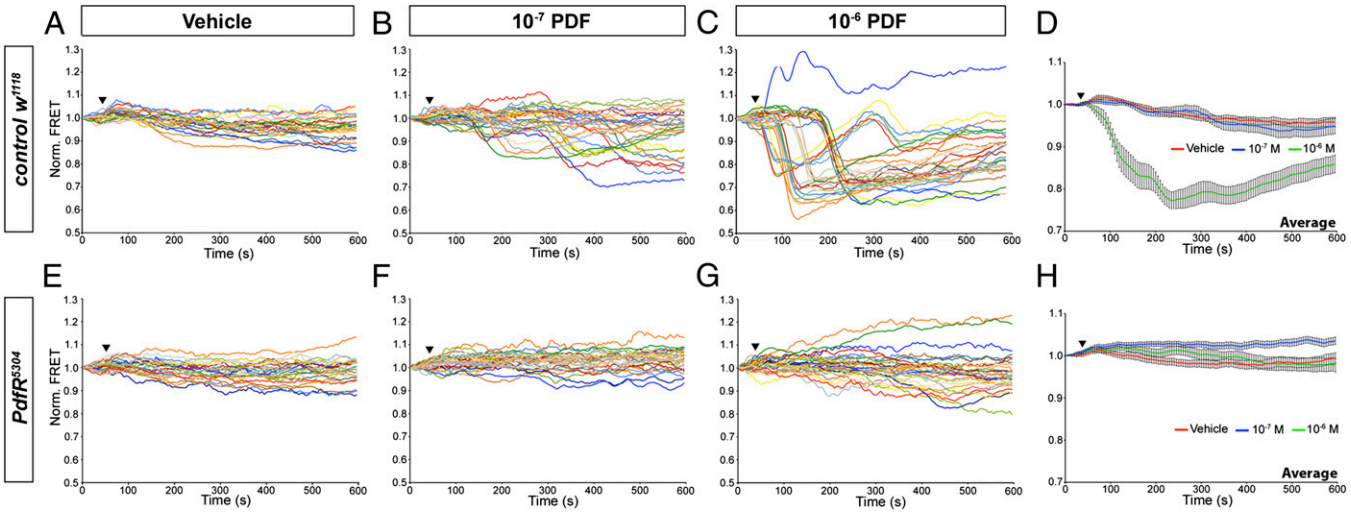

Fig. 4. PDF causes cAMP increases in ureter muscles. Epac1-camps FRET imaged from the ureter muscles of adult male *Drosophila*. Decreases in YFP/CFP FRET indicate increases in cAMP. (*A–C*) The responses of wild-type (w^{1118}) male ureter muscles to vehicle (0.1% DMSO), 10^{-7} M PDF, and 10^{-6} M PDF, respectively. The data for 10^{-6} and 10^{-7} M are based on six ureters from six w^{1118} flies with five regions of interest (ROIs) per ureter. The data for vehicle controls are based on five ureters from five flies with five ROIs per ureter. (*D*) Mean normalized FRET responses for the traces shown in *A–C*. The FRET values for the 10^{-6} M PDF treatment were significantly different from vehicle controls after 110 s ($P < 0.001$). No significant differences were observed between the vehicle and the 10^{-7} M PDF, although several individual muscles responded to this dose (*B*). (*E–G*) Responses of $PdfR^{5304}$ mutant ureter muscles to vehicle, 10^{-7} M PDF, and 10^{-6} M PDF, respectively. The data for the 10^{-6} and 10^{-7} M PDF treatments are based on six ureters from six flies with five ROIs per ureter. The data for vehicle controls are based on five ureters from five flies with five ROIs per ureter. (*H*) The average normalized FRET responses for the traces shown in *E–G*. For $PdfR^{5304}$ ureter muscles, neither peptide dose caused significant FRET changes compared with vehicle. There was a significant difference between $PdfR^{5304}$ and w^{1118} when treated with 10^{-6} M PDF. By 115 s, the FRET ratios of w^{1118} ureter muscles were significantly lower than those of $PdfR^{5304}$ ($P < 0.001$). In graphs *D* and *H* the error bars = SEM calculated from all muscles at each timepoint. Black triangles indicate time of bath application.

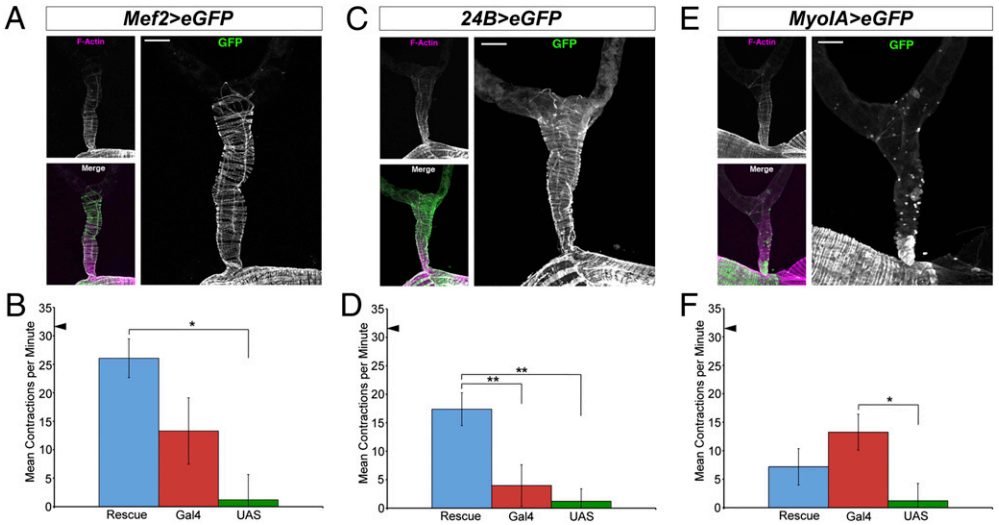

Fig. 5. Ureter muscle expression of PdfR rescues PDF-induced renal contractions in *PdfR* mutants. (*A*) Confocal micrograph of a ureter from a male *w;UAS-eGFP/Mef2-GAL4* fly. (*Upper Left*) Visceral muscle F-actin visualized with fluorescently labeled phalloidin. (*Right*) *GAL4*-driven GFP expression in the ureter. (*Lower Left*) Merged image of phalloidin (magenta) and GFP (green). (*B*) The Mef2 rescue line (*$PdfR^{5304}$;UAS-PdfR/Mef2-GAL4,* shown in blue, $n = 7$) displayed contraction rates in the presence of 10^{-6} M PDF that approached those of PDF-treated Canton S ureters (triangle in *B*). This rescue line showed significantly higher contraction rates than *$PdfR^{5304}$;UAS-PdfR/+* controls (green, $P = 0.0079$, $n = 8$). The Mef2 rescue line also displayed a higher mean ureter contraction rate than *$PdfR^{5304}$;Mef2-GAL4/+;* controls (red, $n = 6$) but because of high contraction rates of a single *$PdfR^{5304}$;Mef2-GAL4/+* preparation, this difference was not statistically significant ($P = 0.0861$). (*C*) A confocal micrograph of a typical ureter from a male *w;UAS-eGFP/+;24B-GAL4/+* fly. Micrographs arranged as for *A*. (*D*) The *24B* rescue line (*$PdfR^{5304}$;UAS-PdfR/+;24B-GAL4/+;* blue, $n = 6$) displayed significantly higher ureter contraction rates in the presence of 10^{-6} M PDF compared with *$PdfR^{5304}$;;24B-GAL4/+;* (red, $P = 0.0087$, $n = 6$) and *$PdfR^{5304}$;UAS-PdfR/+;* (green, $P = 0.0032$, $n = 8$) controls. (*E*) Confocal micrographs of a typical ureter from a male *w;UAS-eGFP/+;MyoIa-GAL4/+* fly revealing expression of *MyoIA-GAL4* in epithelia and a lack of GFP in ureter muscle. Panels arranged as in *A*. (*F*) The frequency of ureter contractions in the presence of 10^{-6} M PDF in the *$PdfR^{5304}$;UAS-PdfR/+;MyoIA-GAL4/+* rescue line (blue, $n = 6$) and the *$PdfR^{5304}$;;MyoIA-GAL4/+* (red, $n = 6$) and *$PdfR^{5304}$;UAS-PdfR/+* (green, $n = 8$) controls. There were no significant differences in ureter contraction rates between the rescue and control lines ($P = 0.2403$ for *GAL4* control and $P = 0.0597$ for *UAS* control). There was a significant difference in contraction rate between the *GAL4* control and the *UAS* control ($P = 0.0051$). (Scale bars, 50 μm in *A*, *C*, and *E*.) Black triangles in *B*, *D*, and *F* represent the frequency of ureter contractions displayed by wild-type Canton S ureters in the presence of 10^{-6} M PDF. For ease of comparison, the same data for *PdfR/UAS-PdfR* controls ($n = 8$) were included on all three histograms. *$P < 0.05$; **$P < 0.01$.

the ureter control the flow of urine into the terminal portion of the digestive tract (29, 30) in a manner analogous to the $VPAC2R^{+}$ detrusor muscle of the mammalian bladder. Abnormal fluid regulation has also been described in mice lacking VIP or PACAP (40, 42, 43), so it will be of interest to establish if PDF signaling has related in vivo roles in flies. The presence of VIP/PACAP immunoreactivity in neural fibers of the lower urinary tract of mammals suggests a local, transmitter-like action on the excretory muscle receptors (12), and VIP is generally believed to act as a local neurotransmitter rather than as a circulating hormone (44, 45). However, systemic effects of gut-derived VIP cannot be ruled out. Indeed, VIP plasma levels increase after an oral osmotic load or intravenous application of cholinesterase inhibitors (46, 47). In light of our findings, which reveal a role for circulating PDF on the renal system, a possible systemic function of VIP deserves further investigation using, for example, transgenic mice lacking the peptide in specific (enteric vs. renal) neuronal populations.

What the Gut Tells the Kidney. Previous work has made use of the larger viscera of locusts or crickets to establish that some neuropeptides induce renal tubule movements (35, 48). Our results using *Drosophila* indicate that renal regulators are secreted from an unexpected source, the gut-innervating ab-PDF neurons, to act as endocrine regulators of the renal muscles, which are entirely devoid of innervation (Fig. 1*C* and Fig. S1) (24). Indeed, our dTrpA1 experiments strongly suggest that the normal ligand for visceral PdfR is released from the gut-innervating ab-PDF neurons, because the only other site of PDF production in mature adults are the clock interneurons in the brain, which are thought to be chemically insulated from the hemolymph by the blood-brain barrier (49) and were not present during our dTrpA1 excitation experiments. Consistent with this idea, extracts of the abdominal ganglia of another insect, *Carausius morosus*, have a potent stimulatory action on renal tubule writhing, the active factors in which were suspected to be peptides (50).

The directionality of this endocrine signal from the gut to the renal system is unexpected and may be of relevance to mammals, where functional links between the digestive and excretory systems are well established with regard to absorption and secretion, and evidence suggests that communication between the two systems might facilitate their concerted action (44). An enterorenal axis, whereby unidentified gut-derived signals affect kidney function

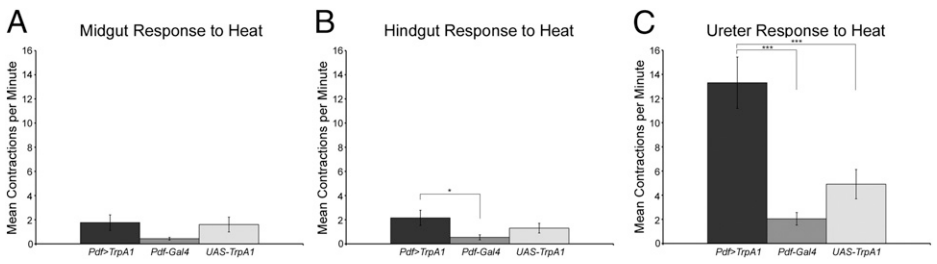

Fig. 6. TrpA1-mediated excitation of ab-PDF neuron axons induces ureter contractions. Following 5 min of incubation at high temperature (31 °C), the contraction rates of explanted midguts (*A*) or hindguts (*B*) were not significantly different between *w; PDF-GAL4/+;UAS-dTrpA1/+* and *GAL4/+* or *UAS/+* controls (for midguts, Friedman rank sum test, $P = 0.004$, asymptotic general independence test, $P = 0.9$, $n = 20$; for hindguts, Friedman rank sum test, $P = 0.002$, asymptotic general independence test, $P = 0.02$, pair-wise comparisons $P = 0.02$ compared with *GAL4* control, $P = 0.3$ compared with *UAS* control, $P = 0.4$ between controls, $n = 20$). (*C*) The same conditions led to a significant increase in the contraction rate of ureters in *w; PDF-GAL4/+;UAS-dTrpA1/+* (Friedman rank sum test, $P < 0.001$, asymptotic general independence test, $P < 0.001$, pair-wise comparisons $P < 0.001$ compared with *GAL4* control, $P < 0.001$ compared with *UAS* control, $P = 0.4$ between controls, $n = 20$). Full genotypes are as follows: *w;PDF-GAL4/+;UAS-dTrpA1/+* (PDF > dTrpA1); *w;PDF-GAL4/+* (*PDF-GAL4*) and *w;; +/UAS-dTrpA1* (*UAS-dTrpA1*). *$P < 0.05$; ***$P < 0.001$.

directly, has recently been proposed on the basis of two observations: the activity of duodenal mucosa homogenates on kidney ion secretion and the differential effect of intravenously versus orally administered sodium loads on renal sodium excretion (44).

In summary, our findings indicate a role for PDF in the control of visceral physiology in the fly, thereby extending the similarities between fly PDF and mammalian VIP beyond their shared role in circadian timekeeping. These findings have also revealed a peptidergic enterorenal axis in *Drosophila*, the evolutionary conservation and significance of which deserves further investigation.

Methods

Fly Stocks and Rearing. A detailed list of fly stocks and a description of fly rearing conditions are described in *SI Methods*.

Imaging, Anatomy, and Physiology. Detailed methods for all imaging, anatomical, and physiological experiments are described in *SI Methods*.

Citations relevant to fly stocks and experimental methods are listed in *SI Methods*.

ACKNOWLEDGMENTS. We thank Helen Skaer and Jeremy Skepper for electron microscopy advice and assistance; Paola Cognigni and Robert Denver for critical reading of the manuscript; Michael Bate and Jimena Berni for the water-heated chamber for the *Drosophila* TrpA1 experiments; Vivek Mehta for conducting the blind quantifications of visceral contraction movies; Katherine Lelito, Ann Marie Macara, Zepeng Yao, and Qi Zhang for assisting with visceral dissections for real-time PCR, and Mohammad Samie for real-time PCR advice and assistance; and Bruce Edgar, Manfred Frasch, Matthias Landgraf, Stefan Pulver, Iris Salecker, Jim Skeath, Ralf Stanewsky, Paul Taghert, the Bloomington Stock Center, and the Developmental Studies Hybridoma Bank. I.M-A. thanks her family for babysitting while she worked on this manuscript. This work was funded by a Wellcome Trust Research Career Development Fellowship WT083559 (to I.M.-A.); National Institutes of Health Grant National Institute of Neurological Disorders and Stroke R00NS62953 (to O.T.S.); a Spanish Ministry of Education fellowship (to D.P.); and a Wellcome Trust doctoral studentship (to G.L.).

1. Field BC, Chaudhri OB, Bloom SR (2010) Bowels control brain: Gut hormones and obesity. *Nat Rev Endocrinol* 6:444–453.
2. Rubino F, R'bibo SL, del Genio F, Mazumdar M, McGraw TE (2010) Metabolic surgery: The role of the gastrointestinal tract in diabetes mellitus. *Nat Rev Endocrinol* 6: 102–109.
3. Johnson LR, ed (2006) *Phsyiology of the Gastrointestinal Tract* (Elsevier Academic, Burlington).
4. Dockray G (1987) Physiology of enteric neuropeptides. *Physiology of the Gastrointestinal Tract*, ed Johnson L (Raven Press, New York), Vol 1, pp 41–66.
5. Schoofs L (1994) Structure, function, and distribution of insect myotropic peptides. *Perspectives in Comparative Endocrinology*, eds Davey KG, Peter RE, Tobe SS (National Research Council of Canada, Ottawa), pp 155–156.
6. Veenstra JA, Agricola HJ, Sellami A (2008) Regulatory peptides in fruit fly midgut. *Cell Tissue Res* 334:499–516.
7. Nässel DR, Winther ÅME (2010) *Drosophila* neuropeptides in regulation of physiology and behavior. *Prog Neurobiol* 92:42–104.
8. Brown BE, Starratt AN (1975) Isolation of proctolin, a myotropic peptide, from *Periplaneta americana*. *J Insect Physiol* 21:1879–1881.
9. Taghert PH, Veenstra JA (2003) *Drosophila* neuropeptide signaling. *Adv Genet* 49:1–65.
10. Vosko AM, Schroeder A, Loh DH, Colwell CS (2007) Vasoactive intestinal peptide and the mammalian circadian system. *Gen Comp Endocrinol* 152:165–175.
11. Reubi JC (2000) In vitro evaluation of VIP/PACAP receptors in healthy and diseased human tissues. Clinical implications. *Ann N Y Acad Sci* 921:1–25.
12. Yoshiyama M, de Groat WC (2008) The role of vasoactive intestinal polypeptide and pituitary adenylate cyclase-activating polypeptide in the neural pathways controlling the lower urinary tract. *J Mol Neurosci* 36:227–240.
13. Nitabach MN, Taghert PH (2008) Organization of the *Drosophila* circadian control circuit. *Curr Biol* 18:R84–R93.
14. Colwell CS, et al. (2003) Disrupted circadian rhythms in VIP- and PHI-deficient mice. *Am J Physiol Regul Integr Comp Physiol* 285:R939–R949.
15. Renn SCP, Park JH, Rosbash M, Hall JC, Taghert PH (1999) A pdf neuropeptide gene mutation and ablation of PDF neurons each cause severe abnormalities of behavioral circadian rhythms in *Drosophila*. *Cell* 99:791–802.
16. Aton SJ, Colwell CS, Harmar AJ, Waschek J, Herzog ED (2005) Vasoactive intestinal polypeptide mediates circadian rhythmicity and synchrony in mammalian clock neurons. *Nat Neurosci* 8:476–483.
17. Brown TM, Colwell CS, Waschek JA, Piggins HD (2007) Disrupted neuronal activity rhythms in the suprachiasmatic nuclei of vasoactive intestinal polypeptide-deficient mice. *J Neurophysiol* 97:2553–2558.
18. Im SH, Li W, Taghert PH (2011) PDFR and CRY signaling converge in a subset of clock neurons to modulate the amplitude and phase of circadian behavior in Drosophila. *PLoS ONE* 6:e18974.
19. Lear BC, Zhang L, Allada R (2009) The neuropeptide PDF acts directly on evening pacemaker neurons to regulate multiple features of circadian behavior. *PLoS Biol* 7:e1000154.
20. Shafer OT, Taghert PH (2009) RNA-interference knockdown of *Drosophila* pigment dispersing factor in neuronal subsets: The anatomical basis of a neuropeptide's circadian functions. *PLoS ONE* 4:e8298.
21. Hyun S, et al. (2005) Drosophila GPCR Han is a receptor for the circadian clock neuropeptide PDF. *Neuron* 48:267–278.
22. Lear BC, et al. (2005) A G protein-coupled receptor, groom-of-PDF, is required for PDF neuron action in circadian behavior. *Neuron* 48:221–227.
23. Mertens I, et al. (2005) PDF receptor signaling in *Drosophila* contributes to both circadian and geotactic behaviors. *Neuron* 48:213–219.
24. Cognigni P, Bailey AP, Miguel-Aliaga I (2011) Enteric neurons and systemic signals couple nutritional and reproductive status with intestinal homeostasis. *Cell Metab* 13:92–104.
25. Nässel DR, Shiga S, Mohrherr CJ, Rao KR (1993) Pigment-dispersing hormone-like peptide in the nervous system of the flies *Phormia* and *Drosophila*: Immunocytochemistry and partial characterization. *J Comp Neurol* 331:183–198.
26. Helfrich-Förster C (1997) Development of pigment-dispersing hormone-immunoreactive neurons in the nervous system of *Drosophila melanogaster*. *J Comp Neurol* 380: 335–354.
27. Miguel-Aliaga I, Thor S (2004) Segment-specific prevention of pioneer neuron apoptosis by cell-autonomous, postmitotic Hox gene activity. *Development* 131: 6093–6105.
28. Spana EP, Kopczynski C, Goodman CS, Doe CQ (1995) Asymmetric localization of numb autonomously determines sibling neuron identity in the Drosophila CNS. *Development* 121:3489–3494.
29. Dow JT, Davies SA (2001) The *Drosophila melanogaster* Malpighian tubule. *Advances in Insect Physiology*, ed Evans PD (Academic, San Diego), pp 1–83.
30. Wessing A, Eichelberg D (1978) Malpighian tubules, rectal papillae and excretion. *The Genetics and Biology of Drosophila*, eds Ashburner M, Wright TRF (Academic, New York), Vol 2c, pp 1–42.
31. Shafer OT, et al. (2008) Widespread receptivity to neuropeptide PDF throughout the neuronal circadian clock network of *Drosophila* revealed by real-time cyclic AMP imaging. *Neuron* 58:223–237.
32. Nikolaev VO, Bünemann M, Hein L, Hannawacker A, Lohse MJ (2004) Novel single chain cAMP sensors for receptor-induced signal propagation. *J Biol Chem* 279: 37215–37218.
33. Ranganayakulu G, Schulz RA, Olson EN (1996) Wingless signaling induces nautilus expression in the ventral mesoderm of the *Drosophila* embryo. *Dev Biol* 176:143–148.
34. de Souza NJ, Dohadwalla AN, Reden J (1983) Forskolin: A labdane diterpenoid with antihypertensive, positive inotropic, platelet aggregation inhibitory, and adenylate cyclase activating properties. *Med Res Rev* 3:201–219.
35. Blake PD, Kay I, Coast GM (1996) Myotropic activity of *Acheta* diuretic peptide on the foregut of the house cricket, *Acheta domesticus* (L.). *J Insect Physiol* 42:1053–1059.
36. Jiang H, Edgar BA (2009) EGFR signaling regulates the proliferation of *Drosophila* adult midgut progenitors. *Development* 136:483–493.
37. Hamada FN, et al. (2008) An internal thermal sensor controlling temperature preference in *Drosophila*. *Nature* 454:217–220.
38. Helfrich-Förster C, Homberg U (1993) Pigment-dispersing hormone-immunoreactive neurons in the nervous system of wild-type *Drosophila melanogaster* and of several mutants with altered circadian rhythmicity. *J Comp Neurol* 337:177–190.
39. Bitar KN, Makhlouf GM (1982) Relaxation of isolated gastric smooth muscle cells by vasoactive intestinal peptide. *Science* 216:531–533.
40. Girard BM, Malley SE, Braas KM, May V, Vizzard MA (2010) PACAP/VIP and receptor characterization in micturition pathways in mice with overexpression of NGF in urothelium. *J Mol Neurosci* 42:378–389.
41. Harmar AJ, et al. (2004) Distribution of the VPAC2 receptor in peripheral tissues of the mouse. *Endocrinology* 145:1203–1210.
42. May V, Vizzard MA (2010) Bladder dysfunction and altered somatic sensitivity in PACAP-/- mice. *J Urol* 183:772–779.
43. Studeny S, et al. (2008) Urinary bladder function and somatic sensitivity in vasoactive intestinal polypeptide (VIP)-/- mice. *J Mol Neurosci* 36:175–187.
44. Michell AR, Debnam ES, Unwin RJ (2008) Regulation of renal function by the gastrointestinal tract: Potential role of gut-derived peptides and hormones. *Annu Rev Physiol* 70:379–403.
45. Unwin RJ, Ganz MD, Sterzel RB (1990) Brain-gut peptides, renal function and cell growth. *Kidney Int* 37:1031–1047.
46. Porter JP, Ganong WF (1982) *Vasoactive Intestinal Peptide. Advances in Peptide Hormone Research* (Raven Press, New York), pp 285–297.
47. Porter JP, Thrasher TN, Said SI, Ganong WF (1985) Vasoactive intestinal peptide in the regulation of renin secretion. *Am J Physiol* 249:F84–F89.
48. Coast GM (1998) The influence of neuropeptides on Malpighian tubule writhing and its significance for excretion. *Peptides* 19:469–480.
49. Carlson SD, Juang JL, Hilgers SL, Garment MB (2000) Blood barriers of the insect. *Annu Rev Entomol* 45:151–174.
50. Pilcher DEM (1971) Stimulation of movements of Malpighian tubules of *Carausius* by pharmacologically active substances and tissue extracts. *J Insect Physiol* 17:463–470.
51. Barolo S, Carver LA, Posakony JW (2000) GFP and beta-galactosidase transformation vectors for promoter/enhancer analysis in *Drosophila*. *Biotechniques* 29:726, 728, 730, 732.

Supporting Information

Talsma et al. 10.1073/pnas.1200247109

SI Methods

Fly Stocks. All crosses and experiments were kept at 25 °C in light-controlled incubators in 12-h:12-h light-dark cycles. Five- to 10-d-old flies were used for all experiments unless otherwise indicated. Flies were raised using a cornmeal/yeast/agar diet [1.2% (vol/vol) autolyzed yeast, 5.5% (vol/vol) cornmeal, 6% (vol/vol) dextrose, 0.55% agar supplemented with 0.18% Nipagin and 2.9 mL/L Propionic acid]. The transgenic lines used in the study were: *PDF-GAL4* (1), $PdfR^{5304}$ and $PdfR^{3369}$ (2), $UAS\text{-}Epac1\text{-}camps^{50A}$ (3), *Mef2-GAL4* (4), *24B-GAL4* (5, 6), $UAS\text{-}PdfR^{16L}$ (7), *MyoIa-GAL4* (8), *UAS-eGFP* (9), *UAS-Stinger* (10), *UAS-mCD8-GFP* (11), and *UAS-dTrpA1* (12). All transgenic flies were used in a $yellow^{+}$ genetic background to prevent physiological phenotypes resulting from absence of *yellow* in intestinal/tubule epithelia. Oregon R (OreR), Canton S or w^{1118} flies were used as control flies.

Fixed Tissue Immunohistochemistry. Adult tissues were dissected, mounted on poly-L-lysine-coated slides and fixed in 4% (wt/vol) paraformaldehyde for 20 min. Subsequent washes and incubations were done in PBS with 0.2% Triton. Tissues were incubated overnight with primary antibody at 4 °C, followed by a 2-h incubation with secondary antibodies at room temperature the next day. Antibodies used were: goat α- GFP (Abcam; 1:2,000), mouse α-nc82 (Developmental Studies Hybridoma Bank; 1:50), mouse anti–pigment-dispensing factor (anti-PDF) propeptide (PDF C7, Developmental Studies Hybridoma Bank; 1:50), and rabbit α-Odd-skipped (13) (1:1,000). Phalloidin-Cy5 or Phalloidin-Alexafluor-633 (Molecular Probes) were used at 1:200. Alexafluor-488-, FITC-, Cy3-, and Cy5-conjugated secondary antibodies were obtained from Jackson Immunolaboratories and used at 1:200 (1:100 for the Cy5-conjugated antibody). All preparations were mounted in Vectashield with or without DAPI (Vectorlabs) and images were acquired using Leica SP5 or Olympus FV1000 confocal microscopes.

Transmission Electron Microscopy. Transmission electron microscopy (TEM) was carried out using standard procedures. Briefly, dissected guts and associated tubules were dissected and fixed overnight in 5% (vol/vol) glutaraldehyde in 0.1 M sodium phosphate buffer at 4 °C. The next day, viscera were postfixed in osmium tetroxide, bulk-stained in 2% (wt/vol) uranylacetate, dehydrated, and embedded in araldyte. Sections were cut at 50–60 nm with a Leica Ultracut UCT and mounted on 100-mesh copper grids. They were double stained with 2% uranylacetate in 50% (vol/vol) methanol followed by lead citrate, and imaged in an FEI Tecnai G2 TEM operated at 120 kv. Images were captured with an AMT XR60B digital camera running Deben software.

Visceral Contraction Measurements Using PDF Peptide. For our initial experiments, flies were anesthetized on ice and adult intestines and their associated Malpighian tubules were dissected into ice-cold Tübingen and Düsseldorf *Drosophila* Ringer's solution containing 46 mM NaCl, 180 mM KCl, 2.2 mM $CaCl_2$, and 10 mM Tris (pH 7.2) using fine forceps and microscissors. The dissected viscera were gently unfurled and stuck to the bottom of a 35-mm Grenier culture dish (Grenier Bio One) under 1.8 mL hemolymph-like saline (HL3) (14) containing 70 mM NaCl, 5 mM KCl, 1.5 mM $CaCl_2$, 20 mM $MgCl_2$, 10 mM $NaHCO_3$, 5 mM trehalose, 115 mM sucrose, and 5 mM Hepes (pH 7.1). Viscera were stuck down on the adherent dish with the Malpighian tubules situated at right angles from the gut (Fig. S2). To ensure that the tubule specificity of PDF's effects was not a result of the use of ice-cold Tübingen and Düsseldorf *Drosophila*, we repeated our bath-applied PDF experiments using CO_2 anesthetization and room temperature HL3 for dissection. These two preparations are referred to as "Cold Ringer's" and "Warm HL3" in the text, figures, and legends.

The small and fragile nature of the *Drosophila* ureter made mechanical recording of its contractions problematic. We therefore used movie recordings of the midgut/hindgut/ureter junction as a means to quantify such contractions. Movies were captured under an Olympus S2 × 7 stereomicroscope fitted with a DP21 CCD camera and control unit (Olympus). Six-minute, 12-s movies, the maximum movie length for the DP21 control unit, were captured for each experiment. Visceral contractions of the guts and ureters were defined as a perceptible constriction of a segment of gut or ureter and recorded visually during movie playback with the observer blind to treatment and genotype. Motility data were expressed as contractions per minute (cpm) by dividing the total number of contractions observed during each 6-min, 12-s movie by 6.2. Ureter and midgut contractions were recorded in independent viewings.

PDF peptide was added as a 200-μL volume of 10× peptide in 1% (vol/vol) DMSO in HL3, yielding a final DMSO concentration of 0.1%. Basal contraction rates were recorded for viscera exposed to neither vehicle nor peptide. Vehicle controls were added as 200-μL volumes of 1% DMSO. For the PDF dose–response curves wild-type male and female (Canton S) flies were dissected and treated as described above with a series of PDF concentrations or vehicle. Movies of PDF- or vehicle-treated viscera were taken starting 5 min after the addition of peptide/vehicle. Dose–response curves were created by a nonlinear regression analysis using the least squares fitting method in Prism 5 for Macintosh (Graphpad). The resulting curves were used to determine EC_{50}s. For the PDF responses of w^{1118} and *PdfR* mutants to 10^{-7} M PDF, 6-min, 12-s baseline movies were recorded before the addition of peptide/vehicle, a second 6-min, 12-s movie was captured 5 min after the addition of peptide/vehicle. We conducted pair-wise comparisons of basal and PDF-treated contraction rates by means of Mann–Whitney *U* tests using Prism 5 (n = 7–10 for each condition).

In Situ Detection of PdfR mRNA. A digoxigenin-labeled PdfR antisense probe was synthesized using RH51443 cDNA as template, and was purified using mini Quick Spin Columns (Roche). Adult visceral tissues were dissected and fixed on poly-L-lysine–coated slides. In situ hybridization was carried out as previously described (15). Samples were prehybridized for 1 h at 58 °C, and were hybridized overnight at the same temperature. Following incubation with an antidigoxigenin antibody conjugated with alkaline phosphatase, colorimetric detection of the probe was performed with the NBT/BCIP substrates. Wild-type and PdfR mutant digestive tracts were simultaneously dissected and processed on the same slide (n = 5 for each genotype).

Real-Time PCR Analysis of Visceral PdfR Expression. Primers for *PdfR* RNA were designed to amplify a 225 base sequence within a *PdfR* exon that is deleted by the $PdfR^{5304}$ mutation. The forward and reverse primers for *PdfR* were TAATGAAGCTGCGTCAATCG and CCTCGCCATTTAGAAAGCAG, respectively. *PdfR* RNA levels were normalized to *Rpl32* RNA, which encodes a ribosomal protein that serves as a convenient housekeeping gene (16). The forward and reverse primers for

Rpl32 were CGGATCGATATGCTAAGCTGT and GCGCTTGTTCGATCCGTA, respectively. The RNA extraction protocol used was previously described (17). Briefly, individual flies were dissected within 2-min windows and tissues of interest were placed into ice cold TRIzol (Invitrogen). All tissues were homogenized within two hours of dissection. RNA was extracted with chloroform (Acros Organics) and precipitated with isopropanol (Sigma-Aldrich). RNase-free conditions were maintained by cleaning all tools and surfaces with Ambion RNaseZap (Invitrogen) and using RNase free solutions. Following extraction, RNA was stored at −20 °C for 3 d or less before it was used for cDNA synthesis, which was performed using the SuperScript III First-Strand Synthesis SuperMix for qRT-PCR kit (Invitrogen). Real-time PCR was performed using ABsolute Blue qPCR SYBR Green Low ROX Mix (Thermo Fisher Scientific) in a 7500 Fast Real-Time PCR System (Applied Biosystems).

cAMP Live-Imaging. Epac1-camps FRET imaging was performed on the cold Ringer's visceral preparation described above using male w^{1118};*Mef2-GAL4*/*UAS-Epac1camps*^{50}; and $PdfR^{5304}$;*Mef2-GAL4*/*UAS-Epac1camps*^{50A} flies. Ureters were imaged with an Olympus FV 1000 scanning laser confocal microscope, through a LUMPL 20×/0.50 water objective with immersion cone and correction collar (Olympus). Frames were scanned once every 5 s with a 440-nm laser using a DM405-440/515 dichroic mirror and CFP/YFP emission was separated by means of a SDM510 dichroic. For each region of interest (ROI), an average spillover-corrected FRET ratio was determined for each time-point by the following equation:

$$\text{Spillover Corrected FRET} = (\text{YFP} - (CFP*0.444))/(\text{CFP}), \quad \textbf{[S1]}$$

where CFP and YFP are the CFP and YPF emission intensities and 0.444 is the proportion of CFP emission spillover into the YFP channel on our imaging system. Using Olympus's Fluoview software, ROIs were selected over individual muscles of a single ureter, making sure to make each ROI large enough to accommodate the movement of the muscle during PDF-induced contractions (Fig. S5). Thus, each ROI contained pixels corresponding to both background Epac1-cAMPs expressing ureter muscle. Confocal apertures for CFP and YPF emission were increased relative to the optimal confocal diameters to increase the thickness of the optical section as an additional means to accommodate the moving ureters. FRET traces were filtered with a six-timepoint moving average, and normalized to the value of the first timepoint (= 1.0). We created average traces in Excel (Microsoft) by calculating the average ratio and SE at each timepoint for each treatment and genotype. Pooled time-courses were compared by means of repeated measures ANOVAs with Bonferroni posttests using Prism 5 for Macintosh (Graphpad). Peptide or vehicle was added as described for the contraction assays above.

***Drosophila* TrpA1 Activation of Visceral PDF Axons.** Flies for this experiment were grown at 18 °C. After eclosion, flies were maintained at 22 °C for 5–8 d and were then transferred (without using CO_2) to room-temperature HL3 buffer, in which their digestive tracts and Malpighian tubules were dissected. Explanted viscera were stuck to the bottom of a 35-mm Grenier culture dish (or Falcon Easy Grip) as described above under visceral contraction measurements. The dish was kept in the dark at room temperature for 10 min, and was then placed onto a 33 °C water-heated Plexiglass chamber for 3 min, until the temperature in the Petri dish had reached 31 °C. Explanted viscera were allowed to stand for another 5 min at 31 °C. Five-minute movies were then captured at 31 °C under a Leica MZ16F stereomicroscope fitted with a Leica DFC420C camera. Visceral contractions and motility data were recorded and annotated, respectively, as described above for visceral contraction measurements. Pooled experiments were tested for normality using the Shapiro–Wilk test. This revealed a requirement for nonparametric analyses and the Friedman rank-sum ANOVA with an asymptotic general independence test and paired-comparisons was using the R statistical environment.

1. Park JH, et al. (2000) Differential regulation of circadian pacemaker output by separate clock genes in *Drosophila*. *Proc Natl Acad Sci USA* 97:3608–3613.
2. Hyun S, et al. (2005) *Drosophila* GPCR Han is a receptor for the circadian clock neuropeptide PDF. *Neuron* 48:267–278.
3. Shafer OT, et al. (2008) Widespread receptivity to neuropeptide PDF throughout the neuronal circadian clock network of *Drosophila* revealed by real-time cyclic AMP imaging. *Neuron* 58:223–237.
4. Ranganayakulu G, Schulz RA, Olson EN (1996) Wingless signaling induces nautilus expression in the ventral mesoderm of the *Drosophila* embryo. *Dev Biol* 176:143–148.
5. Brand AH, Perrimon N (1993) Targeted gene expression as a means of altering cell fates and generating dominant phenotypes. *Development* 118:401–415.
6. Fyrberg C, Becker J, Barthmaier P, Mahaffey J, Fyrberg E (1997) A *Drosophila* muscle-specific gene related to the mouse quaking locus. *Gene* 197:315–323.
7. Mertens I, et al. (2005) PDF receptor signaling in *Drosophila* contributes to both circadian and geotactic behaviors. *Neuron* 48:213–219.
8. Jiang H, Edgar BA (2009) EGFR signaling regulates the proliferation of *Drosophila* adult midgut progenitors. *Development* 136:483–493.
9. Stevaux O, et al. (2002) Distinct mechanisms of E2F regulation by *Drosophila* RBF1 and RBF2. *EMBO J* 21:4927–4937.
10. Barolo S, Carver LA, Posakony JW (2000) GFP and beta-galactosidase transformation vectors for promoter/enhancer analysis in *Drosophila*. *Biotechniques* 29:726, 728, 730, 732.
11. Lee T, Luo L (1999) Mosaic analysis with a repressible cell marker for studies of gene function in neuronal morphogenesis. *Neuron* 22:451–461.
12. Hamada FN, et al. (2008) An internal thermal sensor controlling temperature preference in *Drosophila*. *Nature* 454:217–220.
13. Spana EP, Kopczynski C, Goodman CS, Doe CQ (1995) Asymmetric localization of numb autonomously determines sibling neuron identity in the *Drosophila* CNS. *Development* 121:3489–3494.
14. Stewart BA, Atwood HL, Renger JJ, Wang J, Wu CF (1994) Improved stability of *Drosophila* larval neuromuscular preparations in haemolymph-like physiological solutions. *J Comp Physiol A Neuroethol Sens Neural Behav Physiol* 175:179–191.
15. Tautz D, Pfeifle C (1989) A non-radioactive in situ hybridization method for the localization of specific RNAs in *Drosophila* embryos reveals translational control of the segmentation gene hunchback. *Chromosoma* 98:81–85.
16. Ponton F, Chapuis MP, Pernice M, Sword GA, Simpson SJ (2011) Evaluation of potential reference genes for reverse transcription-qPCR studies of physiological responses in *Drosophila* melanogaster. *J Insect Physiol* 57:840–850.
17. Emery P (2007) *RNA Extraction From Drosophila Heads. Circadian Rhythms: Methods and Protocols, Methods in Molecular Biology*, ed Rosato E (Humana Press, Totowa, NJ), Vol 362, pp 305–307.

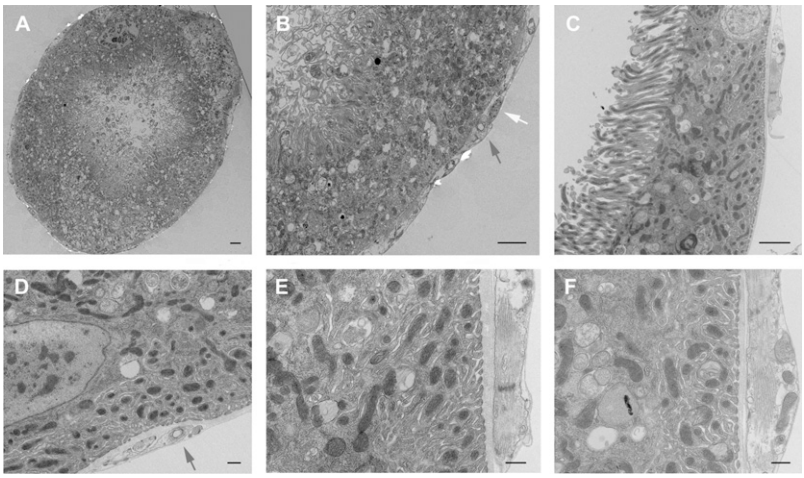

Fig. S1. Transmission electron micrographs of ureter cross-sections reveal its lack of innervation. (*A*) Representative whole ureter cross-sections. (*B*) Two types of cells surround the renal epithelium: visceral muscle cells (white arrow) and trachea (gray arrow). (*C*) Renal epithelial cell with an apical brush border (*Left*). A visceral muscle cell abuts the extracellular matrix on its basal side. (*D*) A tracheal branch (gray arrow) is surrounded by extracellular matrix on the basal side of an epithelial cell, and it is flanked on both sides by visceral muscles. (*E* and *F*) Detail of the basal side of an epithelial cell (*Left*), its basal lamina and a visceral muscle section (*Right*; note the myofilaments in its cytoplasm) in two different ureters. A lack of innervation is indicated by the absence of cytoplasms with the characteristic microtubular ultrastructure of neurons, dense core vesicles, synapses or glial wrappings in all these micrographs. (Scale bars: 2 μm in *A*–*C*; 500 nm in *D*–*F*.)

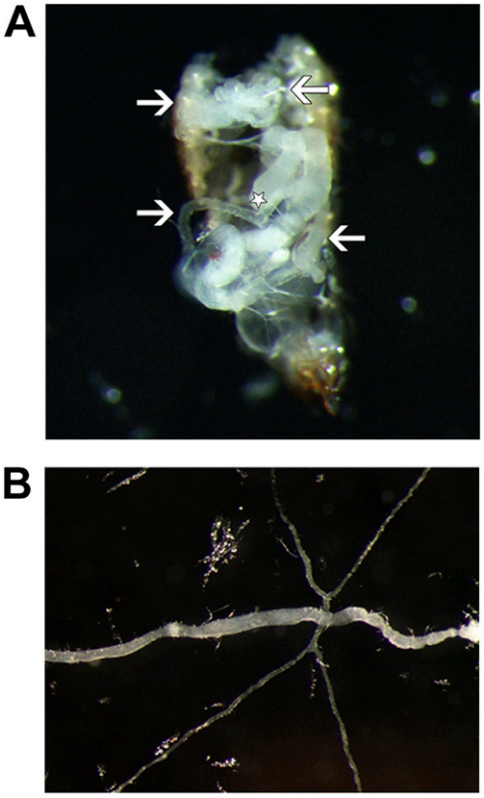

Fig. S2. Preparation of viscera for movie recording. (*A*) Abdomen of a w^{1118} male fly with the ventral cuticle removed before it has been fully dissected. Arrows indicate branches of the Malpighian tubules and the star indicates one of the ureters. Note that one ureter/tubule runs to the anterior portion of the intestine (*Upper* two arrows) and the other is associated with the posterior portion of the intestine and the reproductive organs (*Lower* two arrows). (*B*) An image of w^{1118} male viscera arranged for movie recording. The Malpighian tubules have been dissociated from anterior and posterior viscera and the reproductive organs have been removed. (Magnification: *A*, 5.6×; *B*, 4.5×.)

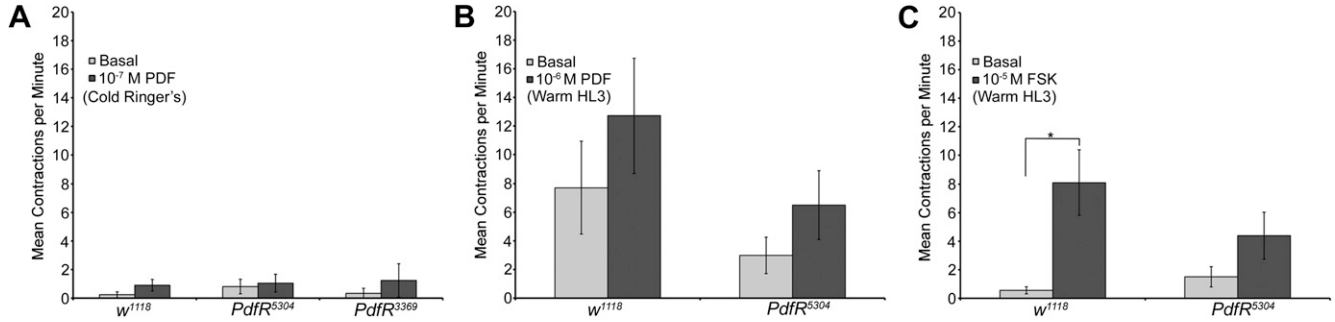

Fig. S3. The effects of PDF and forskolin (FSK) on the rates of midgut contraction in wild-type and *PdfR* mutant viscera. (*A*) Mean basal and PDF-treated (10^{-7} M) midgut contraction rates from viscera dissected from wild-type (w^{1118}) and *PdfR* mutants ($PdfR^{5304}$ and $PdfR^{3369}$) using cold Ringer's (see *SI Methods*). There were no statistically significant differences in basal and PDF-treated midgut contraction rates for any genotype ($P = 0.2500$ for w^{1118}, $P = 0.7500$ for $PdfR^{5304}$, and $P = 0.5000$ for $PdfR^{3369}$). (*B*) Mean basal and PDF-treated (10^{-7} M) midgut contraction rates from viscera dissected from wild-type (w^{1118}) and $PdfR^{5304}$ mutants using warm HL3 (see *SI Methods*). Neither genotype displayed significant differences between basal and PDF-treated contraction rates ($P = 0.2188$ for w^{1118} and $P = 0.1994$ for $PdfR^{5304}$). (*C*) The response of wild-type and $PdfR^{5304}$ mutant midguts to bath-applied FSK from viscera dissected using warm HL3. The midguts of wild-type (w^{1118}) viscera responded to 10 μM FSK with significant increases in contraction rates compared with the basal contraction rates ($P = 0.0151$). Although the mean contraction rate of $PdfR^{5304}$ mutant midguts was slightly higher in the presence of 10 μM FSK, the difference was not statistically significant ($P = 0.1138$). $^*P < 0.05$.

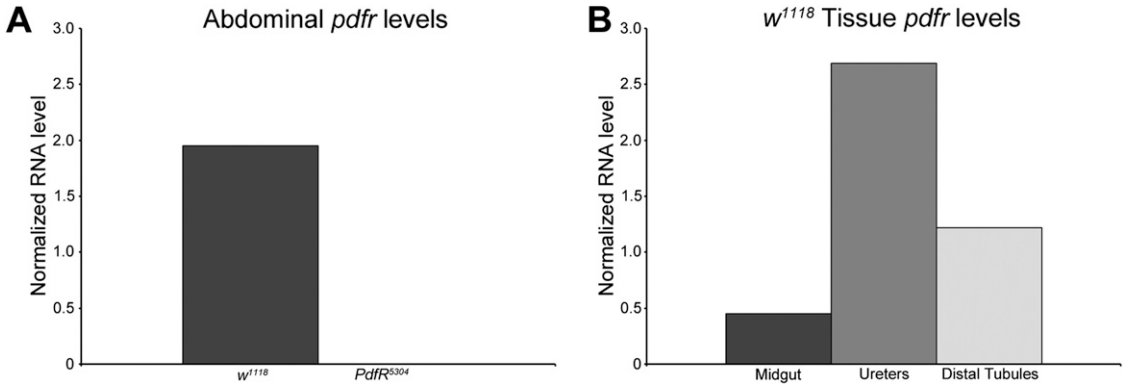

Fig. S4. Real-time PCR analysis of *PdfR* RNA levels in visceral tissues of wild-type flies. (*A*) Comparison of *PdfR* levels from whole abdomen extracts of w^{1118} and $PdfR^{5304}$ flies ($n = 12$ for both). The amount of RNA, normalized to the housekeeping gene *Rpl32,* was negligible in the mutant (0.0029), indicating that the primers designed to amplify a C-terminal region of *PdfR* specifically amplify *PdfR* RNA. (*B*) A comparison of normalized *PdfR* RNA levels in the midguts ($n \sim 70$), ureters ($n \sim 120$), and distal renal tubules ($n \sim 100$) of w^{1118} flies.

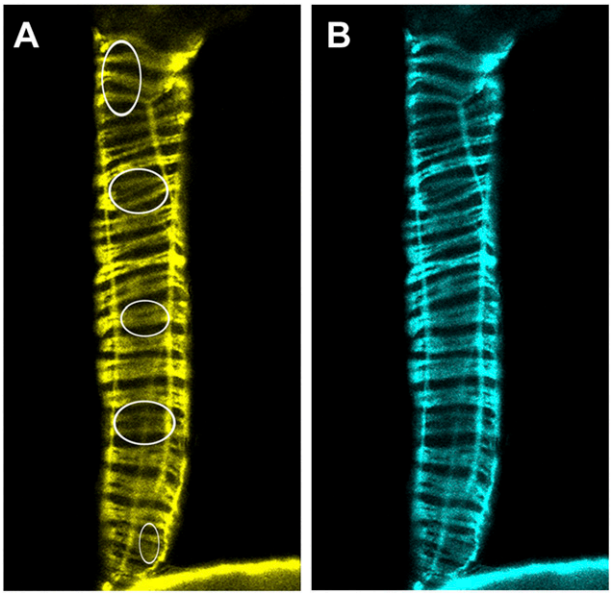

Fig. S5. Epac1-camps expression in the ureter muscles. Images showing YFP (*A*) and CFP (*B*) expression in the ureter of a *w;UAS-Epac1-camps/+;Mef2-GAL4/+* fly. The ovals on the YFP image represent the typical size and distribution of ROIs from which we calculated the change in FRET. The ureter was imaged using a 20× dipping cone objective with a 2× digital zoom.

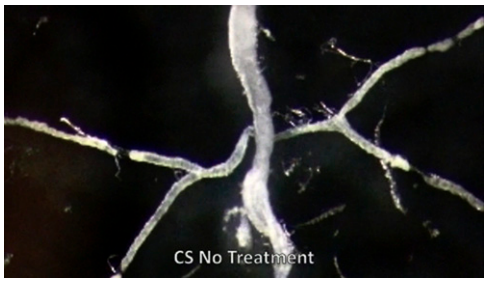

Movie S1. A representative movie of a Canton S intestine that has had no treatment played at 2× speed. (Magnification: 4.5×.)

Movie S1

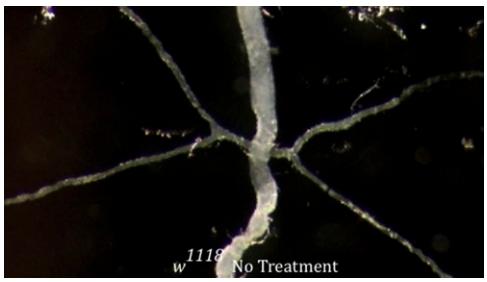

Movie S2. A representative movie of a w^{1118} intestine with no treatment played at 2× speed. (Magnification: 4.5×.)

Movie S2

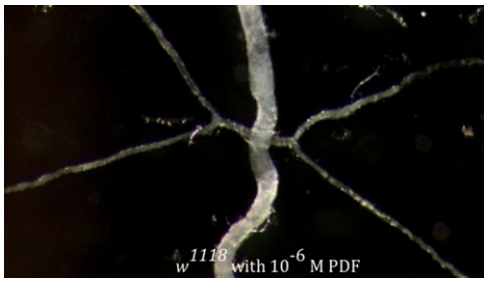

Movie S3. A movie of the intestine from Movie S2, treated with bath applied 10^{-6} M PDF. The movie is also at 2× speed. (Magnification: 4.5×.)

Movie S3

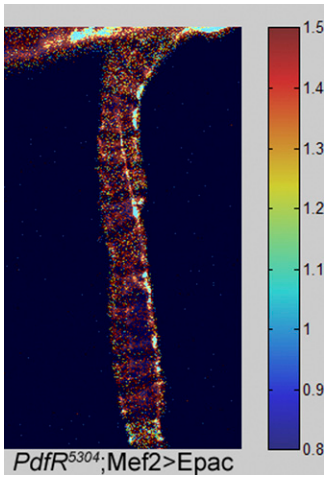

Movie S4. A movie showing the FRET response of *Pdfr*^{5304}*;UAS-Epac1-camps/+;Mef2-GAL4/+* to bath-applied 10^{-6} M PDF. The movie was captured using a 20× dipping cone objective and a 2× digital zoom.

Movie S4

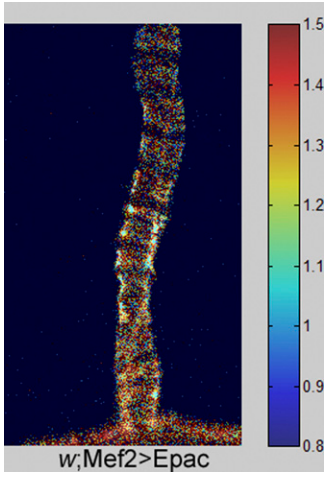

Movie S5. A movie showing the FRET response of *w;UAS-Epac1-camps/+;Mef2-GAL4/+* to bath-applied 10^{-6} M PDF. A decrease in FRET indicates an increase in cAMP. PDF was added in the second second of this 40-s movie (representing about 40 s of actual time). The movie was captured using a 20× dipping cone objective and a 2× digital zoom.

Movie S5

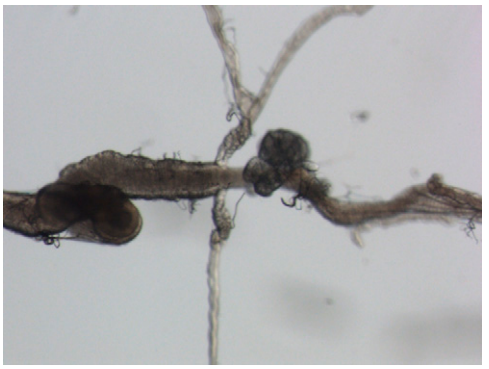

Movie S6. A representative movie of a *UAS-dTrpA1*/+ control intestine 5 min after the shift to 31 °C, played at 2× speed. (Magnification: 8×.)

Movie S6

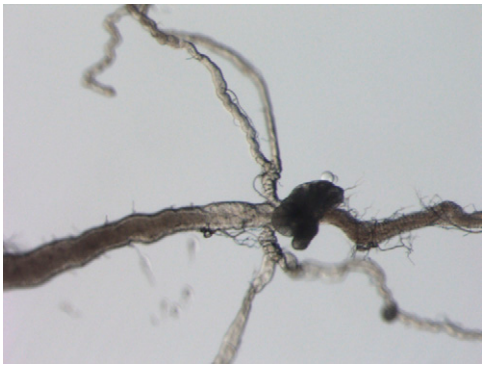

Movie S7. A representative movie of a *PDF* > *dTrpA1* intestine 5 min after the shift to 31 °C, played at 2× speed. (Magnification: 8×.)

Movie S7